**ORIGINAL ARTICLE**

Journal
*American Ceramic Society*

# Hydraulic reactivity and cement formation of baghdadite

Ib Holzmeister[1]  |  Jan Weichhold[1]  |  Jürgen Groll[1]  |  Hala Zreiqat[2]  |  Uwe Gbureck[1]

[1]Department for Functional Materials in Medicine and Dentistry, University of Würzburg, Würzburg, Germany

[2]Biomaterials and Tissue Engineering Research Unit, University of Sydney, Sydney, NSW, Australia

**Correspondence**
Uwe Gbureck, Department for Functional Materials in Medicine and Dentistry, University of Würzburg, Würzburg, Germany.
Email: uwe.gbureck@fmz.uni-wuerzburg.de

**Funding information**
We would also like to acknowledge funding of the crossbeam scanning electron microscope Zeiss CB 340 by the DFG State Major Instrumentation Program (INST 105022/58-1 FUGG).

**Abstract**

In this study, the hydraulic reactivity and cement formation of baghdadite ($Ca_3ZrSi_2O_9$) was investigated. The material was synthesized by sintering a mixture of $CaCO_3$, $SiO_2$, and $ZrO_2$ and then mechanically activated using a planetary mill. This leads to a decrease in particle and crystallite size and a partial amorphization of baghdadite as shown by X-ray powder diffraction (XRD) and laser diffraction measurements. Baghdadite cements were formed by the addition of water at a powder to liquid ratio of 2.0 g/ml. Maximum compressive strengths were found to be ~2 MPa after 3-day setting for a 24-h ground material. Inductively coupled plasma mass spectrometry (ICP-MS) measurements showed an incongruent dissolution profile of set cements with a preferred dissolution of calcium and only marginal release of zirconium ions. Cement formation occurs under alkaline conditions, whereas the unground raw powder leads to a pH of 11.9 during setting, while prolonged grinding increased pH values to approximately 12.3.

**KEYWORDS**

baghdadite, bone cement, hydraulic reactivity, mechanical activation

## 1 | INTRODUCTION

Apart from widely used calcium phosphate ceramics, various calcium and magnesium silicates have been previously investigated as materials for bone replacement, for example, wollastonite ($CaSiO_3$), ackermanite ($Ca_2MgSi_2O_7$),[1,2] diopside ($CaMgSi_2O_6$),[2-4] bredigite ($Ca_7MgSi_4O_{16}$),[2,5] monticellite ($CaMgSiO_4$), merwinite ($Ca_3MgSi_2O_8$), hardystonite ($Ca_2ZnSi_2O_7$),[6] or baghdadite ($Ca_3ZrSi_2O_9$). The materials have been demonstrated not only to be cytocompatible and bioactive but also to direct cellular response to an osteogenic differentiation of mesenchymal stem cells and support vascularization by stimulating angiogenesis.[7] Among the many different calcium silicate phases, baghdadite has shown very promising results not only in vitro[8,9] but also in different animal models.[10-13] The healing process of critical-sized bone defects in both small animal models (rabbit) and big animal models (merino sheep) that were treated

with baghdadite bone grafts could be observed by new bone formation and a significant bridging of ~80% (sheep) or even complete bridging of the radial defect (rabbit) after 12 weeks.[10,11]

In most previous studies, baghdadite was applied as sintered porous ceramic block,[14,15] or partially as a highly porous scaffold in combination with polycaprolactone/nano-bioglas coating to reduce the brittle behavior of the bone graft and to minimize the risk of inflammation.[16] More recently, we were also able to show that baghdadite can also act as a reactive filler compound in acidic setting brushite cement formulations. Here, baghdadite can substitute the ß-tricalcium phosphate (ß-TCP) compound and participate in the setting reaction by delivering $Ca^{2+}$ ions, whereas a calcium-depleted ceramic composed of calcium, zirconium, and silicate is formed.[17] At low baghdadite concentrations, this resulted in a mechanical reinforcement of the cement, whereas at higher concentrations ≥50%, a significant increase in radiopacity was achieved.

Whereas our previous study used a three-component system of baghdadite, ß-TCP, and MCP for cement formation with associated problems such as the need of a homogeneous mixing of all compounds, our current study aimed to produce single-component baghdadite cements. Due to the fact that calcium silicates usually show a hydraulic activity and are widely used in civil engineering Portland cements, we hypothesized that baghdadite may also possess such a hydraulic reactivity and will be able to form self-setting cements. This was investigated in this study by grinding baghdadite for up to 24 h, followed by mixing the resulting powders with water. The setting reaction was analyzed by X-ray diffraction regarding changes of the phase composition as well as mechanical tests to determine the performance under compressive loading.

## 2 | MATERIALS AND METHODS

### 2.1 | Material synthesis

Baghdadite ($Ca_3ZrSi_2O_9$,) was synthesized by mixing zirconium oxide ($ZrO_2$, 45.2 g, Sigma, Darmstadt, Germany), calcium carbonate ($CaCO_3$, 122.3 g, Merck, Germany), silica ($SiO_2$, 49.3 g, Sigma, Germany) in 150-ml isopropanol for 2 h at 200 rpm in a ball mill (Retsch PM400, Haan, Germany). After evaporation of the isopropanol post mixing, the powder mixture was sintered at 1400°C for 3 h, followed crushing with mortar and pestle and sieving <125 μm to obtain a particle size $D_{50}$ of 2.68 ± 0.9 μm. The process of mechanical activation was carried out by further high energy ball-milling of this baghdadite power in isopropanol for 1, 4, and 24 h. Baghdadite cements were obtained by mixing the powders at different milling times with distilled water in a powder to liquid ratio (PLR) of 2 g/ml. The cement pastes were poured into rectangular silicone molds of 12 × 6 × 6 mm and left to set in 100% humidity at 37°C for 3 days.

### 2.2 | Particle size distribution

For each sample, three independent measurements were taken from the different powders to determine the particle size by laser diffraction (LA 300, Horiba, Kyoto, Japan). All powders were suspended in isopropanol and placed for 5 min into an ultrasonic bath prior measurement.

### 2.3 | X-ray diffraction analysis of baghdadite cements

X-ray diffraction measurements were performed with a D8 Advance with DaVinci design (Bruker AXS, Karlsruhe, Germany) at 40 kV and 40 mA. The measurement parameters were set to a 2Theta range of 10°–70°, step size 0.02°, a scan speed of 0.5 s per step and a 0.25° divergence slit. During the measurement, a sample rotation was set to 15 min$^{-1}$. The evaluation tool Diffrac.EVA (Bruker, Germany) was then used to qualitatively determine the phase composition of the cements. With the as obtained XRD measurements, Rietveld refinements and an external standard method called the G-factor method were performed to determine the quantitative phase content.[18] The structures of all phases (ICSD #79453 Baghdadite,[19] ICDD #330302 beta-$C_2S$, ICDD # 270997 $ZnO_2$ cubic, ICDD #371484 $ZnO_2$ monoclinic) determined with Diffrac.EVA were used together with a Chebychev polynomial of the tenth order for the background to refine the parameters scale factor, lattice parameters, crystallite size, and microstrain in the Software Diffrac.TOPAS (Bruker Germany). The values obtained by this refinement were then used to calculate the true crystalline content of the present phases and the amount of amorphous content of the cement via the G-Factor method.

### 2.4 | DTA and TG measurements

For the measurement, the powder was placed in platinum crucibles and measured under an $N_2$ protective gas atmosphere at a flow of 70 ml/min (STA 449 F5 Jupiter Netzsch, Selb, Germany). Data were obtained for a temperature range of 30–1000°C with a heating rate of 20°C/min.

### 2.5 | Compressive mechanical properties

Baghdadite cement pastes were poured into rectangular molds of 12 × 6 × 6 mm and set in the molds at 37°C in 100% humidity for 3 days. A universal testing machine (Roell Z010, Zwick, Ulm, Germany) equipped with a load cell of 10 kN was used for the compressive strength measurement of the cements ($n = 10–12$) at a compression rate of 1 mm/min.

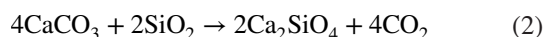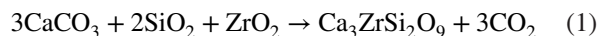### 2.6 | Scanning electron microscopy/energy dispersive X-ray analysis

Cement fragments were coated with a 3-nm platinum layer (ACE600, Leica, Wetzlar, Germany). Scanning electron microscopy (SEM) images were taken with secondary electrons and an acceleration voltage of 2 kV (Crossbeam 340, Zeiss, Oberkochen, Germany). Element maps for calcium, phosphorous, zirconium, oxygen, and silicon were recorded with an energy-dispersive X-ray spectroscope (EDS) (XMaxN, Oxford-Instruments, Wiesbaden, Germany) and evaluated with the attached software AZtec (Oxford-Instruments, Wiesbaden, Germany).

## 2.7 | ICP-MS measurements

Ion concentrations (Ca, Si and Zr) in the used media (MilliQ water & cell culture) were determined using inductively coupled plasma mass spectrometry (iCAP RQ inductively coupled plasma mass spectrometry [ICP-MS], ThermoFisher Scientific, Waltham, USA). Quantitative results for all ions of interest were obtained by measuring against standard solutions with defined concentrations of 5 and 10 mg/L (Merck, Darmstadt, Germany).

## 3 | RESULTS AND DISCUSSION

The synthesis of baghdadite followed the stoichiometric mixture of calcium carbonate, silicon dioxide and zirconium dioxide according to the corresponding ratio of Equation (1). According to Rietveld refinement analysis, the material consisted mainly of baghdadite (95.2%) with minor phases such as zirconium oxide in cubic (1.16%) and monoclinic (1.48%) structure, as well as dicalcium silicate (2.17%). These side phases either stem from remaining raw powder or abrasion of the zirconium oxide milling beaker or may be formed by a side reaction (Equation 2).

$$3CaCO_3 + 2SiO_2 + ZrO_2 \rightarrow Ca_3ZrSi_2O_9 + 3CO_2 \quad (1)$$

$$4CaCO_3 + 2SiO_2 \rightarrow 2Ca_2SiO_4 + 4CO_2 \quad (2)$$

Prolonged grinding of baghdadite was thought to produce a higher amorphous content in the cement powder, which in turn should increase the hydraulic reactivity towards self-setting cement formulations. Such a mechanical activation regime for cement powders is known for a range of different cement types based on calcium silicates,[20] calcium phosphates,[21,22] or magnesium phosphate[23] compounds. Mechanistically, the activation is usually based on a decrease in particle and crystal size, increase in specific surface and increase of the amorphous fraction of the cement powder. All effects result in both a higher rate of dissolution and higher solubility product, which increases the supersaturation level in the cement liquid and hence accelerates cement setting.

As expected, grinding of baghdadite not only resulted in a reduction of particle size $D_{50}$ from $2.68 \pm 0.9\ \mu m$ to $0.59 \pm 0.01\ \mu m$ after 24 h but also lead to decrease of peak intensity and peak broadening in XRD patterns (Figure 1A). The latter is a result of a decrease in crystal size from 150 to 20 nm after 24-h grinding as well as the formation of amorphous domains in the material (Figure 1B). The crystalline and amorphous parts were calculated from XRD measurements using Rietveld refinement combined with an external standard (corundum) method (G-factor). This was done by calculating G with Equation (3), where $S_{cor}$ is the Rietveld scale factor of corundum, $\rho_{cor}$ is the corundum density, $V_{cor}$ as unit-cell volume, $\mu_{cor}^*$ is the mass attenuation coefficient (MAC) of the corundum, and $c_{cor}$ is the weight fraction of corundum. With Equation (4) and this G-factor, it was possible to calculate the amount of crystallinity for each different phase $j$ and additionally the amorphous content in the sample.[18,24] For each phase of the independent XRD measurements, the standard deviation was calculated in the range of 0%–3%. After combing the crystalline calculations of the single phases for each material, the deviation for the amorphous content was 0.00%.

$$G = S_{cor} \frac{\rho_{cor} V_{cor}^2 \mu_{cor}^*}{c_{cor}} \quad (3)$$
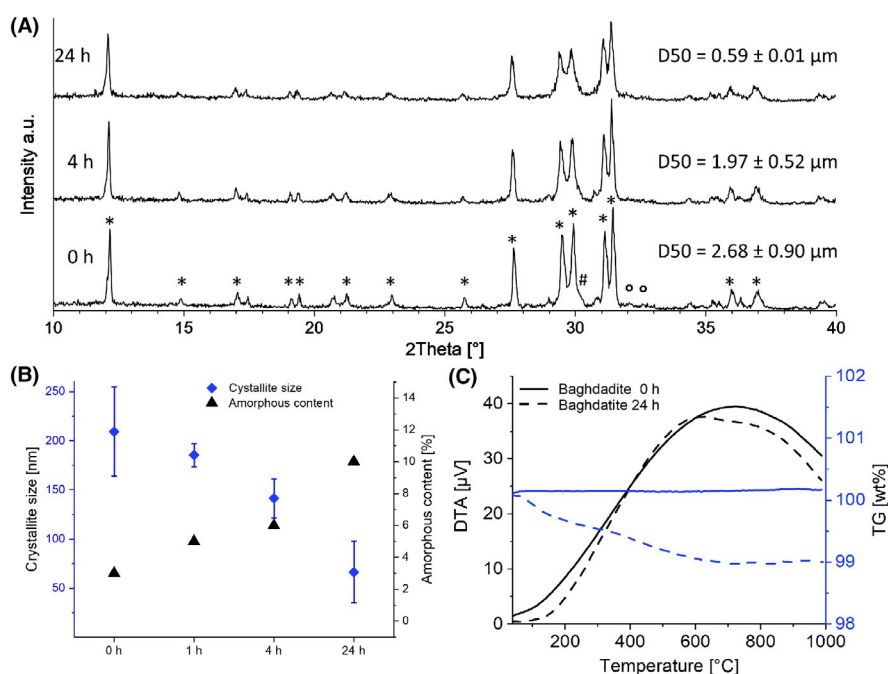


**FIGURE 1** Influence of the grinding time on (A) X-ray diffractograms (* = Baghdadite, # = Zirconoxide, °= C2S) including medium particle sizes, (B) crystal sizes and amorphous content, and (C) differential thermogravimetry and calorimetry of the individual samples. [Color figure can be viewed at wileyonlinelibrary.com]

$$C_j = S_j \frac{\rho_j V_j^2 \mu^*_{\text{sample}}}{G} \quad (4)$$

Although the reduction in crystal size is somewhere following the same trend as for other bioceramics such as α-tricalcium phosphate (α-TCP), the overall amorphization is much less pronounced and reached only 10% after 24 h compared with 71% for α-TCP after a 15 × 15-min grinding regime.[24] This is probably due to the different grinding parameters as well as varying material properties. Hurle et al[24] used 100 balls with a diameter of approx. 10 mm for grinding of 100-g powder, whereas grinding in the current study was performed with 165 balls of 6-mm diameter for 24 h and a change of rotation direction each minute. This likely resulted in a less efficient amorphization as baghdadite particles seemed to have a more brittle character and were predominantly splitted into smaller parts rather than plastically deformed. A similar behavior was found for the calcium magnesium phosphate merwinite,[25] which could be efficiently amorphized by using a 10 times higher rotation speed of the ball mill.

The mechanical activation process could be also seen in differential thermal analysis (DTA)–thermogravimetry (TG) measurements (Figure 1C). The slight loss in mass of the

mechanically activated powder is most likely due to the adsorption of isopropanol on the particle surface because the materials were wet milled and afterwards only dried at ambient conditions.

Activation also influences the solubility of the baghdadite powders as demonstrated by ICP measurements (Figure 2A). The ground powder as well as the set cement was stored in MiliQ water. Practically, all powder showed an incongruent dissolution with an access of dissolved calcium and less released zirconium ions. Although a complete dissolution is expected to lead to a mass ratio of calcium, zircon, and silicon of 2.06:2.56:1.0 in water, solutions with the cement powders were usually depleted regarding Zr and enriched with Ca. The solubility profile of the cement powder showed an increase of Ca and Zr and a decrease of Si in solution. Trends can be determined after 24 h of grinding. The amount of calcium ions in solution increases from ~225 to 325.6 ± 5.01 mg/L (24 h). In a different manner, the concentration of zirconium increases. After no change in solubility until 4 h of milling (~0.1 mg/L), a higher zirconium concentration can be measured for 24 h (1.30 ± 1.64 mg/L). An incongruent trend can be monitored for the silicon release. The solubility of ~4 mg/L without grinding decreases to 3.08 ± 1.61 mg/L after 24-h ball milling. Over the whole grinding time, the
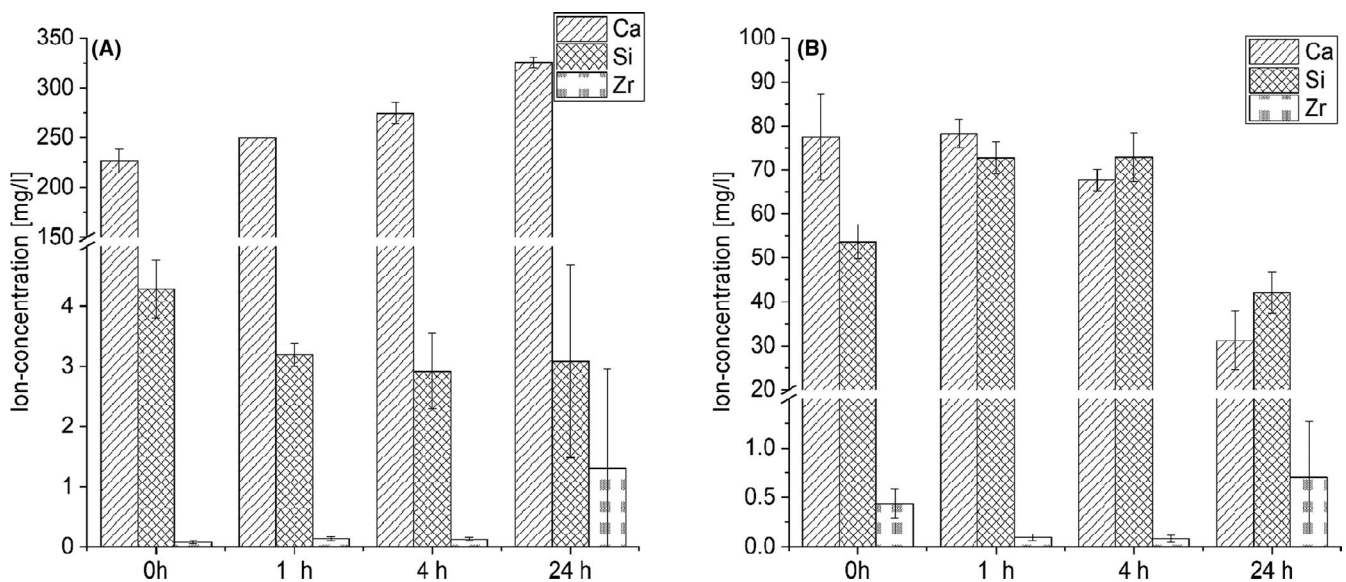


FIGURE 2   Ca, Si, and Zr ion concentrations after 1-day exposure of (A) ground powder in MilliQ water and (B) set cement in MilliQ water.

TABLE 1   Ratios of Ca/Si/Zr ion concentration for solubility testing power and cement in water.

| | Powder in MilliQ water | | | Cement in MilliQ water | | |
|---|---|---|---|---|---|---|
| | Calcium | Silicone | Zircon | Calcium | Silicone | Zircon |
| 0 h | 52.80299 | 1 | 0.017509 | 1.443318 | 1 | 0.008096 |
| 1 h | 78.36963 | 1 | 0.041697 | 1.075463 | 1 | 0.001323 |
| 4 h | 94.03676 | 1 | 0.042163 | 0.928582 | 1 | 0.001113 |
| 24 h | 105.7285 | 1 | 0.42242 | 0.742081 | 1 | 0.016675 |

Ca:Si ratio increased from 52.8:1 (not ground) to 105.7:1 (24-h ground) (Table 1).

In contrast, there is no clear trend for the measurements of the cement samples (Figure 2B), but slight fluctuations can be seen in the different samples. In comparison with the powder samples, it is noticeable that less calcium ions are released, but higher concentrations of silicon ion can be measured. For the zircon ions, no notable changes occur. Noteworthy is the lower Ca/Si ratio, which is in the range of <2:1, which is much nearer to the expected theoretical range.

This increase in solubility also affects the pH value of the cement setting reaction (Figure 3). Whereas the unground baghdadite powder reached a pH plateau of 11.9
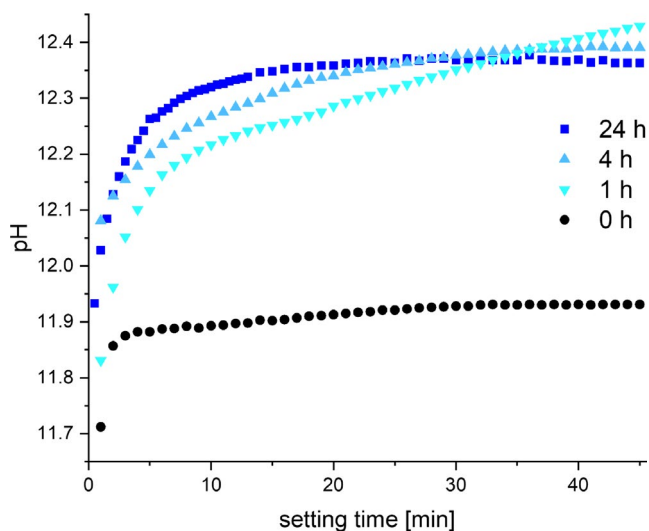


**FIGURE 3** Initial pH changes of the cement setting reaction after mixing the different powders with water. [Color figure can be viewed at wileyonlinelibrary.com]

after 2-3 min, cement pastes made from the ground cement powders resulted in pH ~12.3 after 45-min setting. This corresponds to an increase in $[OH^-]$ by a factor of 2.5 from ~0.0079 to ~0.02 mol\L after 24-h grinding. This increase in pH is somewhere similar to biocements based on tetracalcium phosphate[26] or calcium alkali phosphates,[27] which have been proved to have antimicrobial properties due to their alkaline pH. We would hence speculate that the baghdadite cements from our study could have a similar biological performance regarding their antimicrobial activity.

Mixing of the baghdadite powders with MiliQ water resulted in a hardening of the cement pastes with compressive strengths of up to $1.93 \pm 0.46$ MPa for 24-h ground powder after 3-day setting (Figure 4A). This clearly demonstrated both an inherent hydraulic activity of baghdadite as well as an effect of the grinding regime on the mechanical performance of the cements. How the strength changes over a period of 3 weeks is shown in Figure 4B. The selected sample was the 24-h milled powder. The initial strength value measured after 1 day was only $0.38 \pm 0.07$ MPa, which increased after a setting time of 3 days to $1.93 \pm 0.46$ MPa could be found and later on decreased continuously to ~1 MPa.

These findings were further confirmed by SEM images (Figure 5A), where much larger particles can be seen in the nonground cement, whereas the cement texture becomes more homogeneous with increasing grinding time. In addition, the elemental distribution was affected by grinding as shown for zirconium (Figure 5B), showing a less homogeneous appearance of this element for nonground cements in contrast to a homogeneous distribution for the 24-h ground cement powder.

Surprisingly, XRD measurements of set cements appeared quite similar to the raw powder and did not show the
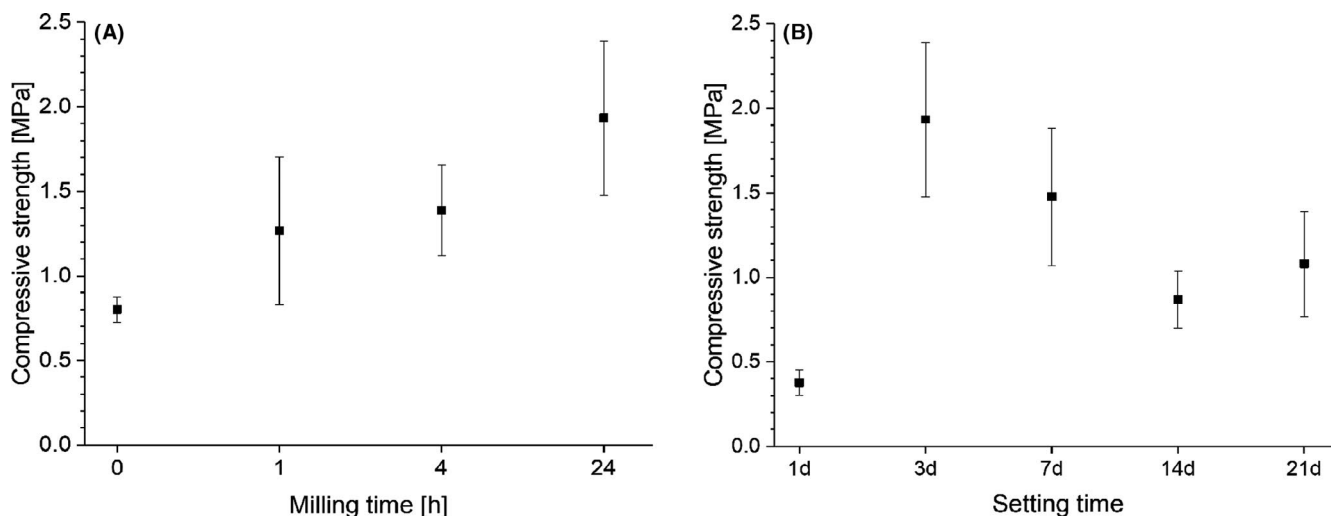


**FIGURE 4** Compressive strength measurements of cement samples with different milling time (A) and 3-week time depending study for hydraulic activity of activated cement (B).
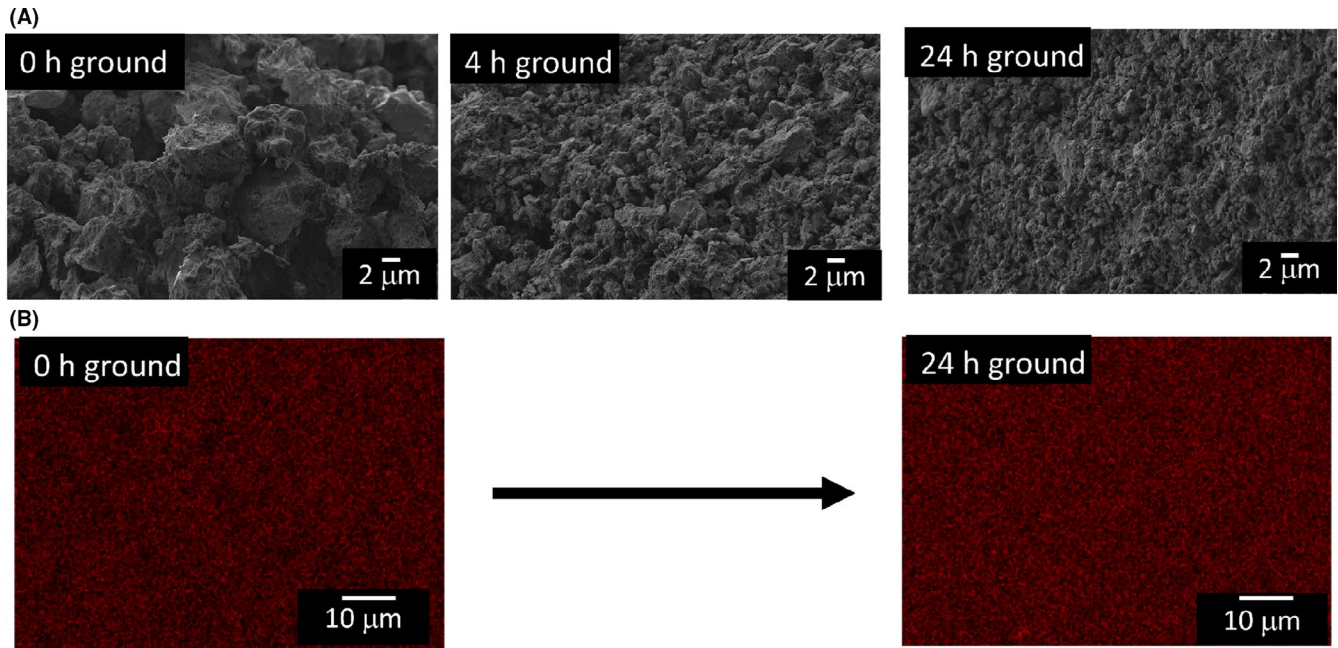
**FIGURE 5** (A) Morphology of baghdadite cements and (B) element mappings for zirconium for baghdadite cements from either unground and 24-h ground cement powders. [Color figure can be viewed at wileyonlinelibrary.com]
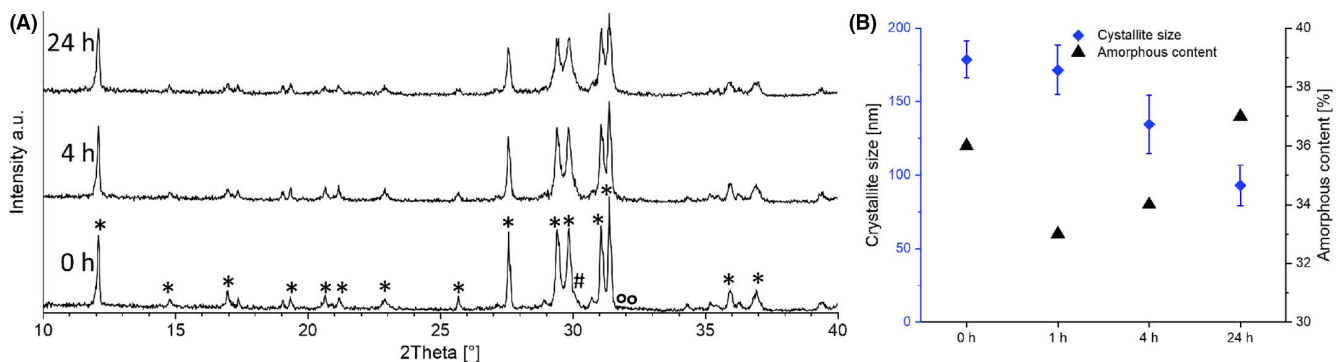


**FIGURE 6** (A) X-ray diffraction patterns (* = Baghdadite, # = Zirconoxide, ° = C2S) and (B) crystal size and calculated amorphous content of baghdadite cements depending on grinding time and setting for 3 days at 37°C. [Color figure can be viewed at wileyonlinelibrary.com]

formation of new crystalline phases (Figure 6A). However, the increase of the amorphous content (Figure 6B) reveals the formation of a noncrystalline setting product, which might consist of hydrated calcium silicates from released $Ca^{2+}$ and $SiO_4^{4-}$ ions:

$$3Ca^{2+} + 2SiO_4^{4-} + 4H_2O \rightarrow Ca_3Si2O_6 \cdot 3H_2O \text{ (CSH)} + 2OH$$
(5)
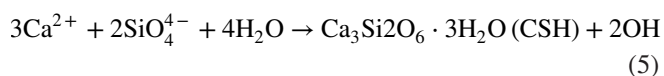
These CSH phases have usually no signals in the XRD due to their amorphous or very weak crystalline character. The reaction of precursors such as $C_3S$ (alite) or $C_2S$ (belite) with water to CSH leads to its substantial material properties, such as greater mechanical strength.[28] The important aspect for the formation of these phases is the Ca/Si ratio. This can range from 1.2 to 2.1. Baghdadite with a Ca/Si ratio of 1.5 is

therefore a potential candidate for the formation of these corresponding CSH phases, even if the value differs a bit from the peculiar optimal ratio of 1.75.[28]

# 4 | CONCLUSION

Baghdadite appears to have an intrinsic hydraulic activity, which can be further enhanced by mechanical activation due to prolonged grinding. This changes the material properties and leads to the formation of amorphous material, which reacts with water to form X-ray amorphous hydrated phases. Although the cements have currently a comparable low mechanical performance of ~2 MPa under compressive loading, strength might be further increased by optimization of the grinding regime leading to

an improved activation process as well as by adjusting a bimodal particle size distribution to increase packing density and reduce cement porosity. Setting of baghdadite occurred without further additives, and baghdadite cements have a clear potential for a biomedical application either in bone replacement or—due to the inherent X-ray opacity[17]—as endodontic filler.

## CONFLICTS OF INTEREST

The authors declare no conflict of interest.

## AUTHOR CONTRIBUTIONS

Conceptualization, I.H. and U.G.; Investigation, I.H. and J.W.; Writing—original draft preparation, I.H.; Writing—review and editing, U.G.; Funding, U.G.

## ORCID

*Uwe Gbureck* https://orcid.org/0000-0002-2584-4176

## REFERENCES

1. Sharafabadi AK, Abdellahi M, Kazemi A, Khandan A, Ozada N. A novel and economical route for synthesizing akermanite (Ca2MgSi2O7) nano-bioceramic. Mater Sci Eng C Mater Biol Appl. 2017;71:1072–8.

2. Wu C, Chang J. Degradation, bioactivity, and cytocompatibility of diopside, akermanite, and bredigite ceramics. J Biomed Mater Res Part B Appl Biomater. 2007;83B(1):153–60.

3. Choudhary R, Vecstaudza J, Krishnamurithy G, Raghavendran HRB, Murali MR, Kamarul T, et al. In-vitro bioactivity, biocompatibility and dissolution studies of diopside prepared from biowaste by using sol-gel combustion method. Mater Sci Eng C Mater Biol Appl. 2016;68:89–100.

4. Wu CT, Ramaswamy Y, Zreiqat H. Porous diopside (CaMgSi2O6) scaffold: A promising bioactive material for bone tissue engineering. Acta Biomater. 2010;6(6):2237–45.

5. Wu CT, Chang J. Synthesis and in vitro bioactivity of bredigite powders. J Biomater Appl. 2007;21(3):251–63.

6. Karamian E, Dehsheikh HG, Hosseini N, Monshi A. An ex vivo comparative study of natural HA/hardystonite nanobiocomposites to use medical applications. J Tissue Eng Regen Med. 2014;8:234.

7. Zhai WY, Lu HX, Wu CT, Chen L, Lin XT, Naoki K, et al. Stimulatory effects of the ionic products from Ca-Mg-Si bioceramics on both osteogenesis and angiogenesis in vitro. Acta Biomater. 2013;9(8):8004–14.

8. Najafinezhad A, Abdellahi M, Ghayour H, Soheily A, Chami A, Khandan A. A comparative study on the synthesis mechanism, bioactivity and mechanical properties of three silicate bioceramics. Mater Sci Eng C. 2017;72:259–67.

9. Graney PL, Roohani-Esfahani S-I, Zreiqat H, Spiller KL. In vitro response of macrophages to ceramic scaffolds used for bone regeneration. J R Soc Interface. 2016;13(120):20160346.

10. Roohani-Esfahani SI, Dunstan CR, Davies B, Pearce S, Williams R, Zreiqat H. Repairing a critical-sized bone defect with highly porous modified and unmodified baghdadite scaffolds. Acta Biomater. 2012;8(11):4162–72.

11. Li JJ, Roohani-Esfahani S-I, Dunstan CR, Quach T, Steck R, Saifzadeh S, et al. Efficacy of novel synthetic bone substitutes in the reconstruction of large segmental bone defects in sheep tibiae. Biomed Mater. 2016;015016.

12. Li JJ, Dunstan CR, Entezari A, Li Q, Steck R, Saifzadeh S, et al. A novel bone substitute with high bioactivity, strength, and porosity for repairing large and load-bearing bone defects. Adv Healthcare Mater. 2019;8(8):1801298.

13. Li JJ, Akey A, Dunstan CR, Vielreicher M, Friedrich O, Bell DC, et al. Effects of material-tissue interactions on bone regeneration outcomes using baghdadite implants in a large animal model. Adv Healthcare Mater. 2018;7(15):1800218.

14. Schumacher TC, Volkmann E, Yilmaz R, Wolf A, Treccani L, Rezwan K. Mechanical evaluation of calcium-zirconium-silicate (baghdadite) obtained by a direct solid-state synthesis route. J Mech Behav Biomed Mater. 2014;34:294–301.

15. Bakhsheshi-Rad HR, Hamzah E, Ismail AF, Aziz M, Hadisi Z, Kashefian M, et al. Novel nanostructured baghdadite-vancomycin scaffolds: In-vitro drug release, antibacterial activity and biocompatibility. Mater Lett. 2017;209:369–72.

16. Sehgal RR, Roohani-Esfahani SI, Zreiqat H, Banerjee R. Nanostructured gellan and xanthan hydrogel depot integrated within a baghdadite scaffold augments bone regeneration. J Tissue Eng Regen Med. 2017;11(4):1195–211.

17. No YJ, Holzmeister I, Lu Z, Prajapati S, Shi J, Gbureck U, et al. Effect of baghdadite substitution on the physicochemical properties of brushite cements. Materials (Basel. Switzerland). 2019;12(10):1719.

18. Jansen D, Stabler C, Goetz-Neunhoeffer F, Dittrich S, Neubauer J. Does Ordinary Portland Cement contain amorphous phase? A quantitative study using an external standard method. Powder Diffrac. 2011;26(1):31–8.

19. Plaister JR, Jansen J, de Graaff RAG, Ijdo DJW. Structure determination of Ca3HfSi2O9 and Ca3ZrSi2O9 from powder diffraction. J Solid State Chem. 1995;115(2):464–8.

20. Mejdoub R, Hammi H, Khitouni M, Sunol JJ, M'Nif A. The effect of prolonged mechanical activation duration on the reactivity of Portland cement: effect of particle size and crystallinity changes. Constr Build Mater. 2017;152:1041–50.

21. Gbureck U, Barralet JE, Radu L, Klinger HG, Thull R. Amorphous alpha-tricalcium phosphate: preparation and aqueous setting reaction. J Am Ceram Soc. 2004;87(6):1126–32.

22. Gbureck U, Hofmann MP, Barralet JE. Thermal performance of mechanically activated tetracalcium phosphate. J Am Ceram Soc. 2005;88(5):1327–30.

23. Brueckner T, Hurle K, Stengele A, Groll J, Gbureck U. Mechanical activation and cement formation of trimagnesium phosphate. J Am Ceram Soc. 2018;101(5):1830–4.

24. Hurle K, Neubauer J, Bohner M, Doebelin N, Goetz-Neunhoeffer F. Effect of amorphous phases during the hydraulic conversion of alpha-TCP into calcium-deficient hydroxyapatite. Acta Biomater. 2014;10(9):3931–41.

25. Kriskova L, Pontikes Y, Cizer Ö, Malfliet A, Dijkmans J, Sels B, et al. Hydraulic behavior of mechanically and chemically activated synthetic merwinite. J Am Ceram Soc. 2014;97(12): 3973–81.

26. Gbureck U, Barralet JE, Hofmann MP, Thull R. Nanocrystalline tetracalcium phosphate cement. J Dent Res. 2004;83(5): 425–8.

27. Gbureck U, Knappe O, Grover LM, Barralet JE. Antimicrobial potency of alkali ion substituted calcium phosphate cements. Biomaterials. 2005;26(34):6880–6.

28. Richardson IG. The calcium silicate hydrates. Cem Concr Res. 2008;38(2):137–58.